BIOCHEMISTRY
including biophysical chemistry & molecular biology
Article

Biochemistry **2009,** *48,* 9393–9404 9393
DOI: 10.1021/bi901177w

The S_0 State of the Water Oxidizing Complex in Photosystem II: pH Dependence of the EPR Split Signal Induction and Mechanistic Implications[†]

Johannes Sjöholm, Kajsa G. V. Havelius, Fikret Mamedov, and Stenbjörn Styring*

Molecular Biomimetics, Department of Photochemistry and Molecular Science, Uppsala University, Ångström Laboratory, P.O. Box 523, S-751 20 Uppsala, Sweden

Received July 10, 2009; Revised Manuscript Received September 7, 2009

ABSTRACT: Water oxidation in photosystem II is catalyzed by the $CaMn_4$ cluster. The electrons extracted from the $CaMn_4$ cluster are transferred to P_{680}^+ via the redox-active tyrosine residue D1-Tyr161 (Y_Z). The oxidation of Y_Z is coupled to a deprotonation creating the neutral radical $Y_Z^\bullet$. Light-induced oxidation of Y_Z is possible down to extreme temperatures. This can be observed as a split EPR signal from $Y_Z^\bullet$ in a magnetic interaction with the $CaMn_4$ cluster, offering a way to probe for Y_Z oxidation in active PSII. Here we have used the split S_0 EPR signal to study the mechanism of Y_Z oxidation at 5 K in the S_0 state. The state of the hydrogen bond between Y_Z and its proposed hydrogen bond partner D1-His190 is investigated by varying the pH. The split S_0 EPR signal was induced by illumination at 5 K between pH 3.9 and pH 9.0. Maximum signal intensity was observed between pH 6 and pH 7. On both the acidic and alkaline sides the signal intensity decreased with the apparent pK_as (pK_{app}) ~4.8 and ~7.9, respectively. The illumination protocol used to induce the split S_0 EPR signal also induces a mixed radical signal in the $g \sim 2$ region. One part of this signal decays with similar kinetics as the split S_0 EPR signal (~3 min, at 5 K) and is easily distinguished from a stable radical originating from Car/Chl. We suggest that this fast-decaying radical originates from $Y_Z^\bullet$. The pH dependence of the light-induced fast-decaying radical was measured in the same pH range as for the split S_0 EPR signal. The pK_{app} for the light-induced fast-decaying radical was identical at acidic pH (~4.8). At alkaline pH the behavior was more complex. Between pH 6.6 and pH 7.7 the signal decreased with pK_{app} ~7.2. However, above pH 7.7 the induction of the radical species was pH independent. We compare our results with the pH dependence of the split S_1 EPR signal induced at 5 K and the $S_0 \rightarrow S_1$ and $S_1 \rightarrow S_2$ transitions at room temperature. The result allows mechanistic conclusions concerning differences between the hydrogen bond pattern around Y_Z in the S_0 and S_1 states.

The light-driven oxidation of water in plants, algae, and cyanobacteria is carried out by the membrane-bound pigment−protein complex photosystem II (PSII)[1]. Upon excitation, P_{680} donates one electron to the primary electron acceptor pheophytin, creating the $P_{680}^+Pheo^-$ charge pair. $Pheo^-$ is oxidized by Q_A, and the electron is transferred via Q_B to the photosynthetic electron transfer chain. Electrons to reduce P_{680}^+ are derived from water, the water oxidation being catalyzed by a $CaMn_4$ cluster in PSII (*1*). The reaction involves four oxidation steps, $S_n \rightarrow S_{n+1}$ ($n = 0-4$), accompanied by the successive removal of four protons from two bound water molecules (*2*, *3*). The electrons from the $CaMn_4$ cluster are transferred to P_{680}^+ via the redox-active tyrosine residue, Y_Z, on the D1 protein. Y_Z is thought to be protonated in its reduced form at physiological pH (*4*, *5*) while the oxidized radical is deprotonated (*6*).

The electron transfer from the $CaMn_4$ cluster to P_{680}^+ involves two sequential steps for each S state transition; first, oxidation of Y_Z by P_{680}^+, to the neutral radical $Y_Z^\bullet$, occurring in the nanosecond to microsecond time scale (*7*−*9*), and second, the oxidation of the $CaMn_4$ cluster by $Y_Z^\bullet$, occurring in the microsecond to millisecond time scale (*10*). The formation of the neutral radical $Y_Z^\bullet$ implies that a deprotonation event of Y_Z-OH is associated with the oxidation of the tyrosine by P_{680}^+. The details in this coupled electron−proton transfer reaction are of importance for the function of Y_Z, and variations of EPT reactions play central roles in several steps associated with the catalytic water oxidation cycle.

It is generally accepted that the phenolic proton of Y_Z moves away in a hydrogen bond to the nearby base D1-His190 (His_Z) when Y_Z is oxidized (*11*, *12*). Upon reduction from the $CaMn_4$ cluster Y_Z is reprotonated. This proton movement has been discussed both in the context of an hydrogen atom abstraction event where an hydrogen atom is abstracted from the $CaMn_4$ cluster upon each S state transition (*6*, *13*, *14*) and in the context of an proton rocking model where the proton moves back and forth between Y_Z and His_Z (*10*, *15*−*18*). In the latter mechanism

[†]The Swedish Research Council, the Swedish Energy Agency, the Nordic Energy Research Project BioH2, and the Knut and Alice Wallenberg Foundation are gratefully acknowledged for financial support.

*Corresponding author: phone, +46 18 471 6580; fax, +46 471 6844; e-mail, stenbjorn.styring@fotomol.uu.se.

[1]Abbreviations: AMPSO, 3-[(1,1-dimethyl-2-hydroxyethyl)amino]-2-hydroxypropanesulfonic acid; Car, carotenoid; Chl, chlorophyll; Cyt b_{559}, cytochrome b_{559}; D1 and D2, the core subunits in PSII; DAD, 3,6-diaminodurene; DMSO, dimethyl sulfoxide; EPR, electron paramagnetic resonance; EPT, coupled electron−proton transfer; HEPES, *N*-(2-hydroxyethyl)piperazine-*N*′-2-ethanesulfonic acid; His_D, histidine 190 on the D2 protein that participates in hydrogen bonding to Y_D; His_Z, histidine 190 on the D1 protein that participates in hydrogen bonding to Y_Z; MES, 2-(*N*-morpholino)ethanesulfonic acid; OEC, oxygen evolving complex; P_{680}, primary electron donor chlorophylls in PSII; pL, pH or pD; P*p*BQ, phenyl-*p*-benzoquinone; PSII, photosystem II; Pheo, pheophytin acceptor in PSII; Q_A and Q_B, primary and secondary plastoquinone acceptors of PSII; S states, intermediates in the cyclic turnover of the OEC; Y_D, tyrosine 161 on the D2 protein; Y_Z, tyrosine 161 on the D1 protein.

© 2009 American Chemical Society
Published on Web 09/08/2009

oxidation of Y_Z facilitates deprotonation reactions in the $CaMn_4$ complex during the S state transitions through electrostatic interactions. Both models involve His_Z to function as an efficient proton acceptor for the proton leaving Y_Z. However, the proton movements to and from His_Z associated with Y_Z oxidation are not necessarily the same in all S states and will certainly vary dependent on pH.

The fast reduction of $Y_Z^\bullet$ by the $CaMn_4$ cluster makes the tyrosine radical short-lived at ambient temperatures and creates obstacles in studying the exact mechanism of Y_Z oxidation. At temperatures above 265 K all S state transitions in the $CaMn_4$ are operational (*19*). By successively lowering the temperature the transitions become inhibited, and below 77 K all S state transitions are blocked. In contrast, it has been demonstrated that light-induced oxidation of a species considered to be Y_Z is still possible at ultralow temperatures (5−10 K) where $Y_Z^\bullet$ cannot be reduced by the $CaMn_4$ cluster. Instead, $Y_Z^\bullet$ is trapped in a semistable state that in most cases decays in the dark on the minutes time scale by recombination with Q_A^- (*20*−*23*). The close proximity of $Y_Z^\bullet$ to the $CaMn_4$ cluster (5.1−5.4 Å) (*24*, *25*) has made it possible to detect this intermediate state by EPR spectroscopy. $Y_Z^\bullet$ is detected as a radical in magnetic interaction with the paramagnetic metal center in OEC (a redox state depicted $S_nY_Z^\bullet$). In PSII, this type of interaction signals, also called "split EPR signals", was first reported from Ca^{2+}-depleted and acetate-inhibited samples (*26*).

The possibility to induce similar split EPR signals by illumination at ultralow temperatures has in recent years brought the advantage to study Y_Z oxidation in intact PSII. Up to now, intermediates of all S states, except the transient S_4 state, have been identified by applying different light regimes (either visible or NIR light) at different low temperatures (for an early review see ref *27*).

Split signal induction is achieved in a large fraction of PSII by visible light illumination at cryogenic temperatures in both the S_0 and S_1 states, giving rise to two characteristic split EPR signals denoted the split S_0 ($S_0Y_Z^\bullet$) and split S_1 ($S_1Y_Z^\bullet$) EPR signals (*20*−*23*, *28*). The signals are estimated to account for ca. 40−50% and ca. 40% of the PSII centers, respectively, when induced at 5−11 K (*20*−*22*). Proton movements and protein conformational changes are severely restricted at these low temperatures. Therefore, if the organic radical involved in the split EPR signals is indeed $Y_Z^\bullet$, the possibility to quite easily oxidize Y_Z implies that the proton movement between Y_Z and His_Z is still operational at this low temperature. This can be probed by studies of split EPR signal induction at 5 K as a function of pH.

The split S_1 EPR signal was found to be pH independent between pH 5.5 and pH 8.5 (*29*). At low pH its formation is inhibited with $pK_a \sim 4.7$ (*29*, *30*). Here we expand these investigations by resolving the pH dependence of the split EPR signal from OEC in the most reduced state, S_0. An explanation for the pH dependence of the split S_0 EPR signal is proposed. Further, we discuss our results in the context of the literature data for the pH dependence of the S state transitions at physiological temperature (*31*, *32*) and the split S_1 EPR signal at 5 K (*29*). This allows mechanistic conclusions concerning differences between the hydrogen bond pattern around Y_Z in the S_0 and S_1 states. Our results also provide further evidence that the radical involved in the split S_0 EPR signal is indeed $Y_Z^\bullet$ and offer insight in structural rearrangements that translate from the donor to the acceptor side of PSII.

MATERIALS AND METHODS

PSII Membrane Preparation. PSII-enriched membranes were prepared from spinach (*Spinacia oleracea*) as in ref *29*. The preparation was kept at −80 °C in a buffer containing 25 mM MES−NaOH (pH 6.1), 15 mM NaCl, 3 mM $MgCl_2$, and 400 mM sucrose. The O_2 evolution was ∼400 μmol of O_2 (mg of Chl)$^{-1}$ h^{-1}, measured under saturating light at 20 °C using 0.5 mM P*p*BQ as an electron acceptor. Tris washing of the samples was achieved by stirring the PSII-enriched membranes in a buffer containing 0.4 M sucrose and 1 M Tris (pH 9.1) at 1 mg of Chl/mL for 30 min on ice under room light. The Tris washing resulted in > 75% removal of Mn from PSII, and no O_2 evolution was detectable after the treatment.

EPR Sample Preparation. PSII membrane preparations were diluted in a standard buffer (25 mM MES−NaOH (pH 6.1), 10 mM NaCl, 10 mM $MgCl_2$, 5 mM $CaCl_2$, and 400 mM sucrose) to 2−3.5 mg of Chl/mL and placed into calibrated EPR tubes. All samples were exposed to room light for 5 min to fully oxidize Y_D and then dark adapted for 30 min. The $CaMn_4$ cluster was synchronized in the S_1 state by giving one preflash and then dark adapted for 15 min at 20 °C (*19*, *28*). The S_0 state was then achieved by giving three saturating turnover laser flashes to the EPR sample which was immediately frozen in a dry ice/ethanol bath (freezing time 1−2 s). Flashes were provided by a Nd:YAG laser (Spectra Physics) at 5 Hz frequency (532 nm, 850 mJ/pulse) at 0 °C. The turnover flashes were given in the presence of 1 mM P*p*BQ (dissolved in DMSO, final DMSO 2% v/v).

For the pH-jump experiments, EPR samples were transferred to a low molar buffering medium (standard buffer but with 0.5 mM MES, pH 6.3) before the preflash protocol. After achieving the S_0 state the buffer was rapidly changed by adding a buffering medium at 150 mM (for the corresponding pH range: pH 3.3−4.25, glutamic acid−NaOH; pH 4.6−6.6, MES−NaOH; pH 6.8−7.8, HEPES−NaOH; pH 8.0−8.7, glycylglycine−NaOH; pH 8.8−9.5, AMPSO) to achieve a final concentration of 20 mM and the desired pH of the sample (*29*, *33*). The samples were frozen within 10 s after the pH adjustment.

pH Reversibility. EPR samples at low and high pH, prepared as described above, were thawed quickly in ethanol after the first EPR measurements, and the pH was changed back to pH ∼6 by adding a 150 mM MES−NaOH buffer to a final concentration of 35 mM (in the low-pH samples) or 30 mM (in the high-pH samples). The samples were mixed and frozen again within 15 s. Parallel samples with only the first pH buffer addition were made in order to determine the obtained pH.

EPR Spectroscopy. Continuous-wave EPR measurements were performed with a Bruker ELEXSYS E500 spectrometer using a SuperX EPR049 microwave bridge and a Bruker SHQ 4122 cavity equipped with an Oxford Instruments cryostat and ITC 503 temperature controller. The split S_0 EPR signal was induced at 5 K by continuous illumination for 90 s from a white light projector filtered through a $CuSO_4$ solution and directed into the cavity via a light guide. The light intensity at the sample position was 20 W/m^2. Signal processing and quantification were carried out with the Bruker Xepr software. Spectrometer settings are given in the figure legends.

Sample Evaluation after pH-Jump Experiments. After the EPR measurements, the remaining oxygen evolution, the final pH, and the Chl concentration of the EPR samples were measured as in refs *29* and *33*. All samples were diluted back to pH 6.1 in a standard buffer within 20 s after each sample was

thawed and the steady-state O_2 evolution was measured. Despite fast sample handling, the $CaMn_4$ cluster might sustain pH-induced damage in a fraction of the centers leading to partial loss of oxygen evolution. This damage is pH and time dependent, occurring faster at extreme pH (*33*). In samples where the activity was slightly lowered, the data points (EPR signal amplitudes) were corrected to full activity. In this way irreversible split EPR signal loss due to pH induced damage of PSII or the OEC could be removed from the analysis. Samples with less than 50% of the original oxygen evolution were judged to be too destroyed to provide reliable data and were excluded. In addition, in the particular EPR sample, EPR signal amplitudes were normalized to the found Chl concentration, which could vary somewhat between the samples due to the elaborate sample preparation protocol.

The bell-shaped titration curves for the split S_0 EPR signal and the fast-decaying radical were fitted with the combination of two pK_as as described in ref *33*. In addition, apparent pK_a values (pK_{app}) are also presented. The pK_{app} corresponds to the pH at which the EPR signal has lost 50% of its maximal amplitude. The pK_{app} values are useful in PSII research since many processes and phenomena can only be partially resolved over limited pH intervals. Often, this makes it impossible to obtain a full titration curve. Therefore, the pK_{app} values, as we use them here, are more relevant to allow comparisons to many of the pK_a values reported in literature, e.g., refs (*30*−*32*). In particular, this holds for many processes on the donor side of PSII which exhibit single pK_a behavior. In those cases our pK_{app} can be directly compared with the determined pK_a which does not hold for the pK_a obtained from the fitting.

RESULTS

pH Dependence of the Split S_0 EPR Signal. The formation of the split S_0 EPR signal induced by illumination at 5 K was investigated between pH 3.9 and pH 9.0. The OEC, synchronized in the S_1 state, was advanced to the S_0 state by three powerful laser flashes given at pH 6.3. Approximately 55% of PSII was in the S_0 state in our samples (*34*). The pH was then immediately altered before the samples were frozen. Changing the pH only *after* the OEC reached the S_0 state excludes any effects by pH on the transitions from S_1 to S_0.

Figure 1A shows the light-induced split S_0 EPR signal at five different pHs. The signal reaches its maximum between pH 6 and pH 7. Spectrum c (pH 6.6) clearly shows the symmetrical features of the signal previously assigned to $S_0Y_Z^{\bullet}$ (*21*), with a low-field peak at $g \sim 2.05$ and a high-field trough at $g \sim 1.96$ separated by ca. 160 G. The amplitude decreases on both the acidic and alkaline sides and is significantly smaller at extreme pHs. In Figure 1B (filled circles) the normalized signal amplitude of the split S_0 EPR signal is plotted against the pH. The signal amplitude is measured on the wing of the low-field peak at 3205 G (indicated by the dashed line in Figure 1A) to eliminate contribution from the split S_3 EPR signal that overlaps the split S_0 EPR signal at the high-field trough (*23*). The maximal observable signal amplitude, measured at pH 6.6, is considered to reflect the formation of the split S_0 EPR signal in 46−53% of the centers that were in the S_0 state (*22*). In Figure 1B this amplitude is set as 100%. The titration curve is fitted with the combination of the two pK_as, 6.2 ± 0.4 and 6.5 ± 0.4. However, in order to facilitate comparison to reported literature values (see Materials and Methods), we will discuss pK_a values obtained from the half-inhibition of the signal amplitude, resulting in the pK_{app}s ~4.8 and ~7.9.

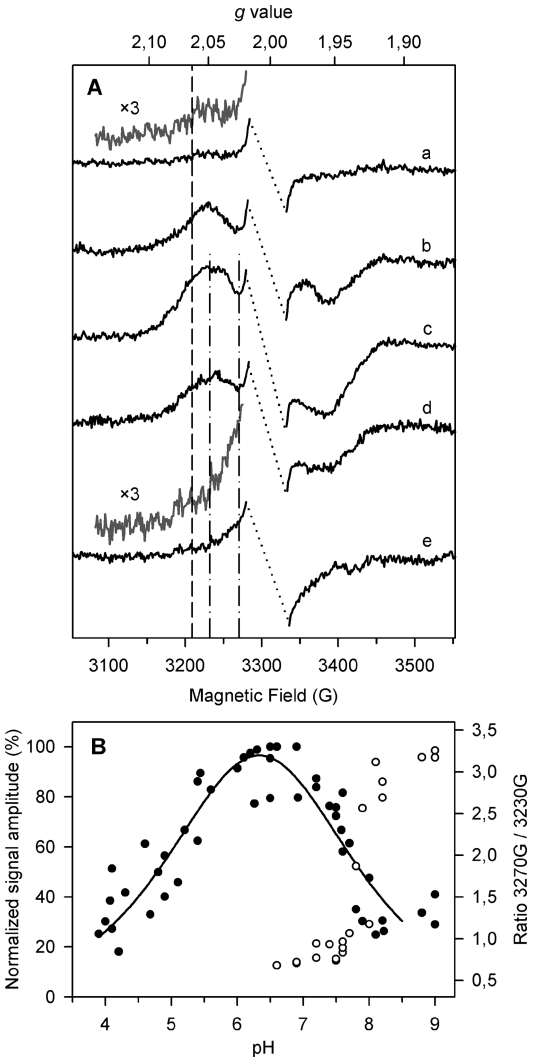

FIGURE 1: pH effect on the split S_0 EPR signal induced by illumination at 5 K. (A) The split S_0 EPR signal in light minus dark difference spectra measured at different pHs: (a) pH 4.2, (b) pH 4.9, (c) pH 6.6, (d) pH 7.6, and (e) pH 8.1. The central region of the spectra containing the radical part has been omitted for clarity. The dashed line at 3205 G indicates the field position chosen for the amplitude measurements presented in panel B. EPR parameters: temperature 5 K, microwave frequency 9.41 GHz, microwave power 25 mW, and modulation amplitude 10 G. (B) Filled circles show the normalized amplitudes of the split S_0 EPR signal vs pH. The pH-dependent behavior of the split S_0 EPR signal could be fitted with a combination of two protonable groups (full drawn line). Open circles show the ratio between the normalized signal amplitudes at 3270 and 3230 G at pHs above 6.6. These field positions are indicated by dash-dot lines in panel A.

The shifts to extreme pHs also result in the appearance of new light-induced EPR signals in the same spectral range. At acidic pH, the peak at $g \sim 2.05$ and trough at $g \sim 1.96$ decrease in amplitude, resulting in an ~19 G broad radical at $g \sim 2.00$ becoming dominant in the EPR spectrum (Figure 1A, spectrum a). At alkaline pH > 7.7 the peak and trough from the split S_0 EPR signal decrease, but here a new resonance appears broadening the $g \sim 2.00$ radical (Figure 1A, spectrum e). This new light-induced EPR feature decays in the dark with $t_{1/2} \sim 3$ min (not shown) and is also a fast relaxing signal similar to the split S_0 EPR signal (*23*). To evaluate this new EPR feature that

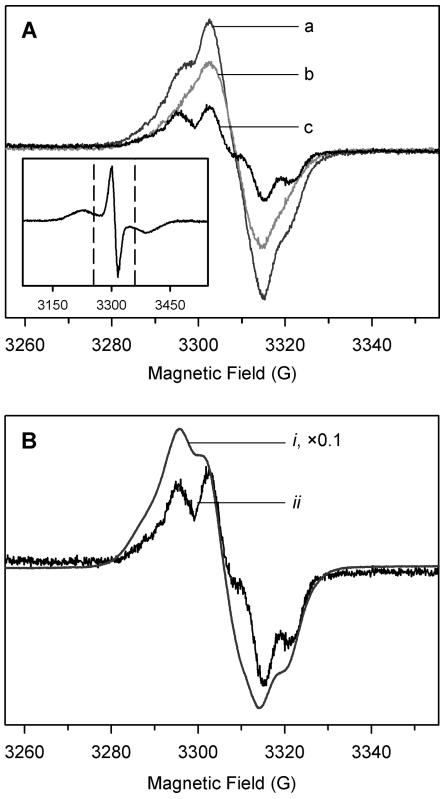

FIGURE 2: Induction of radical EPR signals at pH 6.1 in the $g \sim 2$ region by illumination at 5 K of a three-flash sample dominated by the S_0 state. (A) Spectrum a shows the light minus dark difference EPR spectrum induced by illumination at 5 K. Spectrum b shows the part of the light-induced EPR signal that remained after 15 min incubation in the dark. Spectrum c shows the light-induced signal that decayed during these 15 min in the dark at 5 K. Spectrum c was obtained by subtraction of spectrum b from spectrum a. The inset spectrum shows the entire light-induced spectrum recorded as in Figure 1. The dashed lines in the inset spectrum indicate the field region of the radical spectra in Figure 2 in relation to the split S_0 EPR signal. EPR parameters: temperature 5 K, microwave frequency 9.41 GHz, microwave power 1 mW (inset spectrum 25 mW), and modulation amplitude 3.2 G (inset spectrum 10 G). (B) Comparison between the spectrum of $Y_D^{\bullet}$ (i) and the light-induced decaying radical EPR spectrum (ii, same as spectrum c in panel A) both recorded at 1 mW microwave power. Note the difference in scale and spectral resolution. EPR parameters are the same as in panel A.

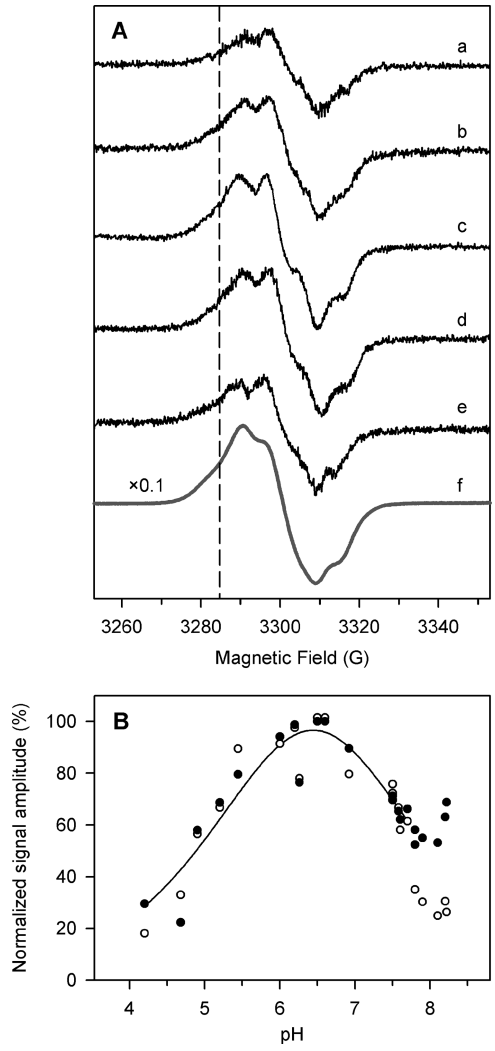

FIGURE 3: pH effect on the light-induced, fast-decaying radical EPR signal from PSII in the S_0 state. (A) The decaying radical EPR spectrum at different pHs: (a) pH 4.2, (b) pH 4.9, (c) pH 6.6, (d) pH 7.6, and (e) pH 8.1. The difference spectra shown are obtained by subtracting the spectra recorded after 9 min incubation in the dark at 5 K from the spectra recorded during illumination. Spectrum f shows the EPR signal of $Y_D^{\bullet}$ measured with the same EPR settings for comparison. EPR parameters; temperature 5 K, microwave frequency 9.41 GHz, microwave power 1 mW, and modulation amplitude 3.2 G. (B) Filled circles show the pH dependence of the normalized amplitude of the decaying radical EPR spectrum measured at 3285 G (dashed line in panel A). The decrease of the amplitude at low and high pH could be fitted between pH 4.2 and pH 7.7 with two protonable groups (full drawn line). Open circles show the normalized amplitude of the split S_0 EPR signal measured in the same samples.

appears at pH > 7.7, the ratio between the EPR signal amplitude at 3270 and 3230 G (Figure 1A, dash-dot lines) was calculated. The ratio changes from smaller than 1 at pH < 7.7 to become larger than 3 at elevated pH, indicating a $pK_{app} \sim 8$ for the appearance of this new broad $g \sim 2$ signal (Figure 1B, open circles).

pH Dependence of the Light-Induced Fast-Decaying g ~ 2 Radical. The light minus dark subtraction spectra in Figure 1 also result in a mixed radical spectrum in the $g \sim 2$ region besides the typical wide symmetrical feature of the split S_0 EPR signal (see also ref *23*). In Figure 1 the spectral conditions are chosen to optimize the "split" features of the EPR spectrum (at 3230 and 3380 G) and to allow observation of the broadening at high pH while we have omitted the central part. This is instead shown in Figures 2 and 3 where the radical region is recorded (under optimal conditions) from samples in the S_0 state illuminated at 5 K at different pHs. The EPR spectrum obtained by illumination at 5 K of a sample at pH 6.1 is shown in Figure 2A (spectrum a). The EPR spectrum is of mixed origin, and it was previously shown that one fraction of the light-induced signal in the central region has the same decay kinetics as the split S_0 EPR signal and involves recombination with Q_A^- (*23*). The remaining part was a slowly decaying radical ($t_{1/2}$ > 30 min) assigned to a $Car^{+\bullet}$ or $Chl^{+\bullet}$ species.

We analyzed the mixed EPR spectra obtained by illumination at 5 K at the different pHs with this in mind. When the illumination is stopped, the split signal and part of the radical species recombine with Q_A^- and decay with a half-time of approximately 3 min (*23*). After 15 min decay of these species a slowly decaying narrow radical signal (line width ~ 12 G) with $g \sim 2.0032$ (Figure 2A, spectrum b) remained. The line width and *g*-value differ from what is reported for $Car^{+\bullet}$ (g = 2.0024, line width 9.5 G) and $Chl^{+\bullet}$ (g = 2.0026, line width 10.4 G) (*35*).

Table 1: pH-Dependent Inhibition of S State Transitions at Room Temperature (RT), Split EPR Signal Formations at 5 K, and the Fast-Decaying Radical at 5 K

	acidic pK_a[a]	alkaline pK_a[a]	ref[a]
$S_0 \rightarrow S_1$, RT	4.7	pH independent	(*31*, *32*)
split S_0, 5 K	4.8[b] [4.7]	7.9[b] [7.7]	this work [*30*]
radical S_0, 5 K	4.8[b]	7.2;[b] pH independent at pH >7.7	this work
$S_1 \rightarrow S_2$, RT	pH independent	pH independent	(*31*, *32*)
split S_1, 5 K	4.7 [4.9]	pH independent [7.7]	*29*, [*30*]

[a]Values in square brackets originate from references in square brackets. [b]pK_{app} (see Materials and Methods).

However, when recording the spectrum under conditions that are nonsaturating for $Car^{+\bullet}/Chl^{+\bullet}$, the slowly decaying radical had $g \sim 2.0027$ and line width ~ 10 G (see below). This concludes that the slowly decaying narrow radical signal that is left after 15 min decay (Figure 2A, spectrum b) is dominated by $Car^{+\bullet}/Chl^{+\bullet}$. By subtracting the slowly decaying radical part ($g \sim 2.0032$) from the mixed radical spectrum recorded during illumination, the contribution from the fast-decaying signal was revealed (Figure 2A, spectrum c). The fast-decaying radical spectrum is ~19.5 G wide with a $g \sim 2.0041$. This *g*-value is significantly higher than for the slowly decaying $Car^{+\bullet}/Chl^{+\bullet}$ ($g \sim 2.0024-26$) (*35*) and is more similar to that of the well-known tyrosine radicals from Y_D and Y_Z ($g \sim 2.0046$) (*36*). In fact, when analyzing the decaying radical spectrum after only 1.5 min decay, it has $g \sim 2.0046$, identical to that of $Y_D^{\bullet}$ and $Y_Z^{\bullet}$. The lower *g*-value, $g \sim 2.0041$, after 15 min decay indicates that this spectrum (Figure 2A, spectrum c) also contained a decaying, very small fraction of a $Car^{+\bullet}/Chl^{+\bullet}$ radical (ref *37*; F. Ho, personal communication).

In Figure 2B, the fast-decaying radical spectrum (spectrum ii) is shown together with the spectrum of $Y_D^{\bullet}$ (spectrum i) recorded under similar conditions. At 5 K and 1 mW microwave power the EPR spectrum from $Y_D^{\bullet}$ is distorted due to rapid passage effects reflecting its slow relaxation (*38*). This is different from the fast-decaying radical that is better resolved. This directly indicates that the fast-decaying radical relaxes faster than $Y_D^{\bullet}$ at 5 K (see below). The size of the fast-decaying radical indicates that it is present in ~5% of PSII at pH 6.1. This approximation is based on double integration of the spectrum (measured under nonsaturating conditions) and comparing its size to the spectrum of $Y_D^{\bullet}$ which accounts to one spin per PSII center.

Figure 3A shows spectra of the fast-decaying radical at five different pH values. The spectra shown are obtained by subtracting the spectra after 9 min decay in the dark from the light-induced signal. The largest spectrum was observed at pH 6.6 (Figure 3A, spectrum c). The signal intensity decreased on both the acidic and the alkaline side. In Figure 3B (filled circles) the normalized signal amplitude measured at 3285 G[2] (indicated by a dashed line in Figure 3A) is plotted against the pH. As a comparison the split S_0 EPR signal amplitude, measured in the same samples, is also shown in Figure 3B (open circles). A titration curve for the fast-decaying radical could be fitted for two protonable groups with the pK_as 5.9 ± 0.4 and 7.1 ± 0.4 (in the pH interval pH 4.2−7.7), while the amplitude was pH independent at pH >7.7. The pK_{app} (see Materials and Methods) obtained from the half-inhibition of the signal amplitude was 4.8 in the acidic region. Thus, at the low-pH side, the split S_0 EPR signal and the fast-decaying radical decreased in concert (pK_{app} ~ 4.8).

[2]The amplitudes were measured at the wing of the EPR spectrum to avoid contributions from any contaminating radical signal from oxidized Chl or Car species.

In the alkaline region the behavior was more complex. Between pH 6.6 and pH 7.7 the signal decreases in size to approximately 60% of its maximal amplitude at pH 6.6. The pK_{app} for this decrease was ~7.2. However, above pH 7.7 the induction of the radical species was pH independent. This is different from the behavior of the split S_0 EPR signal, which decreased to 28% at pH 8.2 (Figure 3B, open circles). We conclude that the fast-decaying radical decreases with the same pH dependence as the split S_0 EPR signal between pH 6.6 and pH 7.7 but has a different pH dependence at pH 7.7−8.2. This is an important difference, and the implications are discussed below.

Table 1 shows the obtained results for the pH dependence of the split S_0 EPR signal and the fast-decaying radical. The table also summarizes previously reported pK_a values for the induction of the split EPR signals in the S_0 and S_1 states and for the inhibition of the room temperature transitions from $S_0 \rightarrow S_1$ and $S_1 \rightarrow S_2$.

Oxidation of Side Path Donors. Our low-temperature illumination protocol also induced a slowly decaying radical species (Figure 2, spectrum b). This featureless radical EPR signal is ~10 G wide with $g \sim 2.0027$ when recorded under nonsaturating conditions (0.5 μW; Figure 4). Judging by the spectral resemblance and its slow decay, this light-induced species predominantly originates from an oxidized Car or Chl radical species in PSII (*35*). The induction of this radical EPR signal was also pH dependent. Figure 4A, spectrum b, shows the slowly decaying radical at pH 6.3. At this pH the radical was formed in ~13% of PSII centers by our illumination regime. The number of reaction centers where Car/Chl was oxidized increased on both the low- and high-pH side. At pH 4.1 and 8.2 the radical was formed in ~19% (Figure 4A, spectrum a) and ~17% (Figure 4A, spectrum c) of PSII, respectively. The quantification of the stable radical was done by comparing the $Car^{+\bullet}/Chl^{+\bullet}$ signal with the signal of $Y_D^{\bullet}$. Figure 4C (closed circles) shows the amount of $Car^{+\bullet}/Chl^{+\bullet}$ formation by our illumination protocol at 5 K between pH 3.9 and pH 8.5. The induction of the radical has a minimum at pH 5.5−7 and increases slightly at both low and high pH. Thus, Car/Chl oxidation is minimum at pHs where the split S_0 EPR signal and the decaying radical are highest and vice versa. Where we found lower yield of the fast-decaying species the yield of the $Car^{+\bullet}/Chl^{+\bullet}$ was higher.

In addition, we also quantified the amount of Cyt b_{559} that was oxidized by our 5 K illumination. Figure 4B shows the spectrum of Cyt b_{559} prior to illumination (spectrum i) in comparison to the spectrum after the illumination at 5 K (spectrum ii). At pH 6.5 the light-induced Cyt b_{559} oxidation was estimated to ~17% (on a PSII basis). The quantification is based on the assumption that the maximally inducible Cyt b_{559} oxidation (Figure 4B, spectrum iii) amounts to one spin per PSII (100%). A fully oxidized sample could be achieved by continuous illumination with our light source for ~80 min at 5 K. For the oxidation of Cyt b_{559} we found

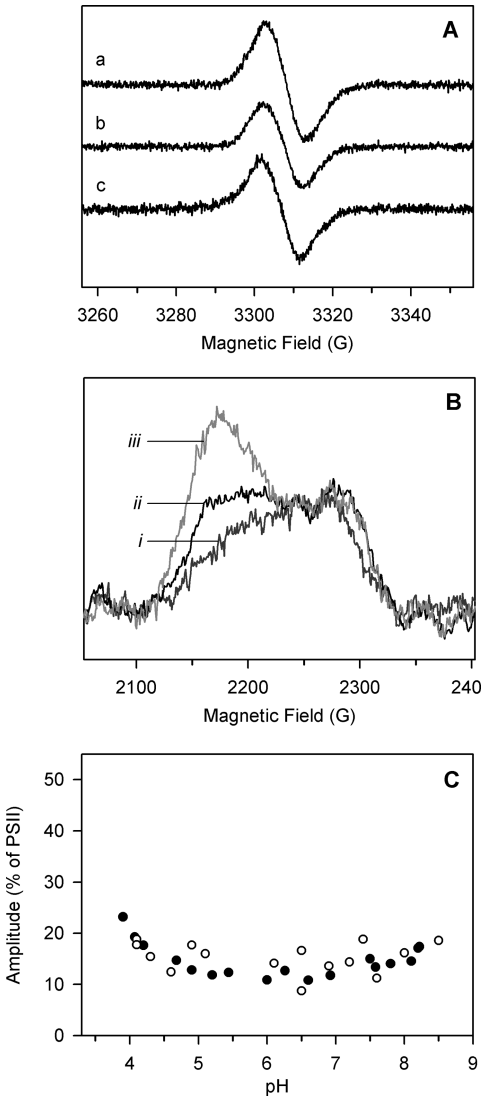

FIGURE 4: pH effects on the induction of the Car/Chl radical and Cyt b_{559} oxidation by illumination at 5 K. (A) The EPR spectra of the slowly decaying light-induced radical attributed to oxidized Car/Chl at three different pH values: (a) pH 4.1, (b) 6.3, and (c) 8.2. EPR parameters: temperature 5 K, microwave frequency 9.41 GHz, microwave power 0.5 μW, and modulation amplitude 3.2 G. (B) The EPR spectra of oxidized Cyt b_{559} before illumination (i), after split signal illumination at 5 K (ii), and after maximal oxidation of Cyt b_{559} by illumination for ~80 min at 5 K (iii). EPR parameters: temperature 15 K, microwave frequency 9.41 GHz, microwave power 5 mW, and modulation amplitude 15 G. (C) The amount of oxidized Car/Chl radical (filled circles) and Cyt b_{559} (open circles) induced by illumination at 5 K between pH 3.9 and pH 8.5. The size of the Car/Chl radical was quantified by comparing the double integration of the Car/Chl signal and the signal of $Y_D^{\bullet}$.

a slightly lower yield at pHs where the induction of the split S_0 EPR signal and the fast-decaying radical was maximal (Figure 4C, open circles).

pH Reversibility. The change to low and high pH significantly decreases both the split S_0 EPR signal and the fast-decaying radical. We therefore designed an experiment to test if the decrease was reversible or not. After the first EPR measurements, samples at low and high pH were thawed, and the pH was changed back to normal pH (pH ~6) by adding additional pH buffer. The black spectrum a in Figure 5A shows the split S_0 EPR signal at pH 4.3. At this pH the characteristic peak and trough of the split S_0 EPR signal are hardly visible (compare to Figure 1).

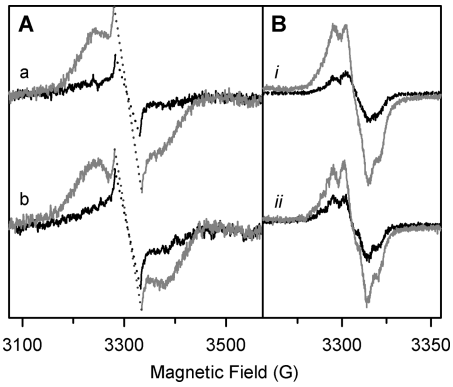

FIGURE 5: Reversibility of the pH-induced decrease of the split S_0 EPR signal and the fast-decaying radical at low and high pH. (A) Spectra a show the split S_0 EPR signal induced by illumination at 5 K at pH 4.3 (black line) and after the same sample has been thawed and the pH changed to 5.9 (gray line). Spectra b show the split S_0 EPR signal induced by illumination at 5 K at pH 7.8 (black line) and after the sample has been thawed and the pH changed to pH 6.2 (gray line). (B) Spectra i show the fast-decaying radical induced by illumination at 5 K at pH 4.3 (black line) and after the sample has been thawed and the pH changed to 5.9 (gray line). Spectra ii show the fast-decaying radical induced by illumination at 5 K at pH 7.8 (black line) and after the same sample has been thawed and the pH changed to pH 6.2 (gray line). EPR parameters are the same as in Figure 1 for panel A and Figure 3 for panel B.

After the pH was changed back to pH 5.9, the second EPR measurement clearly showed that a split S_0 EPR signal could be induced by illumination at 5 K (gray spectrum a in Figure 5A). A similar increase in the split S_0 EPR signal was observed when changing the pH from 7.8 to 6.2 (Figure 5A, black and gray spectra b, respectively). Also, the size of the fast-decaying radical was significantly increased by a change from pH 4.3 to pH 5.9 (Figure 5B, i) and pH 7.8 to pH 6.2 (Figure 5B, ii). It is clear that the protonation/deprotonation events causing the decrease of the split S_0 EPR signal and the fast-decaying radical are reversible when the pH is changed back from extreme pH to normal pH at both the acidic and alkaline sides.

Decay Kinetics of the Split S_0 EPR Signal. The decay of the split S_0 EPR signal at different pHs was followed for 15 min at 5 K after the low-temperature illumination. In Figure 6A the decay of the signal amplitude is shown at three different pH values. The signals decay with similar kinetics ($t_{1/2} \sim 3$ min) at pH 4.6 (filled circles), pH 6.1 (open circles), and pH 7.6 (filled triangles) in agreement with an earlier report (*30*).

Magnetic Relaxation Properties. Figure 6B shows the microwave power saturation behavior of the split S_0 EPR signal, the fast-decaying radical, and $Y_D^{\bullet}$ at pH 6.1. To facilitate comparison, the signal amplitudes have been normalized. For the split S_0 EPR signal and the fast-decaying radical, which both decay after light induction, each point in Figure 6B represents measurements in a separate EPR sample. For the split S_0 EPR signal the change in amplitude at 3205 G was measured between 0.13 and 202 mW. The power at half-saturation, $P_{1/2}$, was derived as in ref *39* and was found to be 19 mW.

The signal amplitude of the fast-decaying radical in samples provided three flashes was measured at 5 K at 3285 G (see Figure 2B) over microwave powers ranging from 1.6 μW to 16 mW. The $P_{1/2}$ was 300 μW at pH 6.1 (Figure 6B, Table 2). In addition, the microwave power saturation of the fast-decaying radical was also determined at pH 7.6, with a $P_{1/2}$ of 360 μW (Table 2).

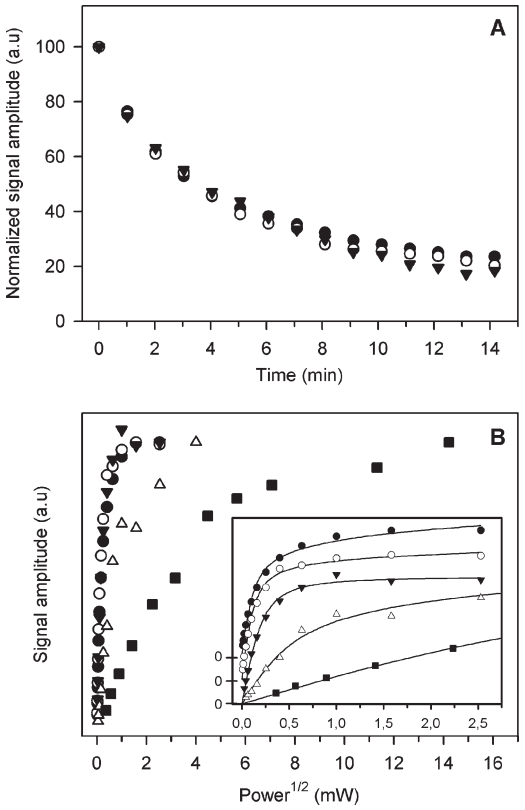

FIGURE 6: (A) Decay kinetics of the split S_0 EPR signal at different pH. The split S_0 EPR signal was induced by illumination at 5 K, and the decay of its amplitude was followed during incubation in the dark at 5 K at different pHs. The amplitude was measured at 3205 G (see Figure 1A) at pH 4.6 (filled circles), pH 6.1 (open circles), and pH 7.6 (filled triangles). EPR parameters are as in Figure 1. (B) Microwave power saturation at 5 K for the split S_0 EPR signal (filled squares), the fast-decaying radical (open triangles), $Y_D^\bullet$ in the dark-adapted sample (open circles), $Y_D^\bullet$ in the sample provided three flashes (filled triangles), and $Y_D^\bullet$ in a Mn-depleted (Tris-washed) sample (filled circles), measured at pH 6.1. The $P_{1/2}$ values were calculated from the fits shown in the inset and are summarized in Table 2. The EPR signal intensities have been normalized to the same maximal amplitude. In the inset, the amplitudes of $Y_D^\bullet$ in the zero-flash, three-flash, and Mn-depleted sample have been separated vertically for clarity. EPR settings were as in Figure 1 for the split S_0 EPR signal and Figure 2 for the fast-decaying radical and $Y_D^\bullet$ except for the microwave power, which varied.

The signal amplitude of $Y_D^\bullet$ on the peak at 3290 G (see Figure 3A) was measured between 0.1 μW and 6.4 mW in three different samples, a zero-flash (S_1 state), a three-flash (S_0 state dominating), and a Tris-washed EPR sample lacking the Mn cluster. $P_{1/2}$ was found to be 19, 57, and 17 μW for $Y_D^\bullet$ in the zero-flash, three-flash, and a Tris-washed EPR sample, respectively. Although measured for the first time at 5 K, these numbers are well in line with earlier data where the S state dependent relaxation of $Y_D^\bullet$ was originally reported (*38*). Also, in this report $Y_D^\bullet$ was found to relax faster in three-flash (S_0 dominated) samples than in dark-adapted (S_1) or Mn-depleted (Tris-washed) PSII samples when measured at 8 and 20 K.

The $P_{1/2}$ of the fast-decaying radical is significantly higher than of $Y_D^\bullet$ (Table 2), indicating that this radical relaxes much faster. Due to this fast relaxation the resolution of the EPR spectra of the fast-decaying radical in Figures 2 and 3 is high even at 1 mW microwave power, and the rapid passage effects that decrease the resolution of the $Y_D^\bullet$ EPR spectrum ((*38*); see Figure 2B) are minimized. It is tempting to attribute the fast-decaying radical to

Table 2: Microwave Power Saturation Behavior of the Fast-Decaying Radical, the Split S_0 EPR Signal, and $Y_D^\bullet$ at pH 6.1

	$P_{1/2}$[a]	
EPR signal	pH 6.1	pH 7.6
fast-decaying radical	300 μW	360 μW
$Y_D^\bullet$ (0 flash)	19 μW	
$Y_D^\bullet$ (3 flashes)	57 μW	
$Y_D^\bullet$ (Tris-washed)	17 μW	
split S_0	19 mW	

[a]Measured at 5 K.

$Y_Z^\bullet$. The relaxation properties of $Y_Z^\bullet$ are expected to be different from $Y_D^\bullet$ as it is influenced by the environment. $Y_Z^\bullet$ relaxation is strongly enhanced by the magnetic interaction with the close-lying $CaMn_4$ cluster, whereas the EPR signal of $Y_D^\bullet$ saturates more easily although also this radical interacts with the $CaMn_4$ cluster (that is > 30 Å away). It was previously shown that a well-resolved transient EPR signal from $Y_Z^\bullet$ can be induced by illumination in Ca^{2+}-depleted PSII, on top of the dark stable $Y_D^\bullet$ signal, when measuring at high microwave powers (*40*). Similar to reported here, it was possible to discriminate between the $Y_Z^\bullet$ and $Y_D^\bullet$ EPR signals using microwave power saturation studies.

DISCUSSION

The oxidation of Y_Z is coupled to a proton movement between the hydroxyl group of the tyrosine and a nearby base. Under physiological conditions this base is believed to be His_Z (*11*, *12*), 2.7 Å away from Y_Z (*25*). The oxidation of Y_Z has been studied here in the S_0 state between pH 3.9 and pH 9.0 at ultralow temperature (i.e., 5 K). As a probe, the light-induced split S_0 EPR signal was used. This signal arises from a magnetic interaction between the oxidized $Y_Z^\bullet$ radical ($S = {}^1/_2$) and the $S = {}^1/_2$ of the $CaMn_4$ cluster in the S_0 state (*41*). The split S_0 EPR signal is a symmetrically broadened EPR spectrum with a peak to trough distance of 160 G centered around $g \sim 2$ (*21*). In addition to the split S_0 EPR signal, a fast-decaying radical was induced in the $g \sim 2$ region, over the same pH interval. We assign this fast-decaying radical to $Y_Z^\bullet$ based on the following: (i) the shape and width (19.5 G) of the EPR signal and its g-value ($g \sim 2.0041-2.0046$) are matching that of a tyrosine radical (Figure 2), (ii) the relaxation of the EPR signal is markedly different from that of $Y_D^\bullet$ (Table 2), and (iii) the signal decays with similar kinetics ($t_{1/2} \sim 3$ min) as the split S_0 EPR signal (*23*). The fast-decaying radical is observed in ca. 5% of the PSII centers at pH 6.5, and the spectral feature of its EPR signal shows no obvious magnetic interaction with the $CaMn_4$ cluster. However, the signal is not from PSII centers lacking the $CaMn_4$ cluster since the power saturation measurements indicate that the closely lying $CaMn_4$ cluster enhances the relaxation properties of the radical (Table 2). The spin−lattice relaxation of $Y_Z^\bullet$ and $Y_D^\bullet$ is expected to be quite similar in samples lacking the $CaMn_4$ cluster (*42*). Instead, we propose that the light-induced, fast-decaying radical signal originates from PSII centers where $Y_Z^\bullet$ is uncoupled and therefore its EPR spectrum is not broadened from magnetic interaction with the $S = {}^1/_2$ of the $CaMn_4$ cluster. At this point we do not speculate further about the mechanism behind this uncoupling. However, we point out that such uncoupling has been reported in temperature dependence studies of split EPR signals involving $Y_Z^\bullet$ and the $CaMn_4$ cluster (*43*, *44*).

Scheme 1: pH-Induced Changes in Y_Z and S_0 Oxidation Triggered by Protonation of His_Z in the Y_Z-His_Z Motif

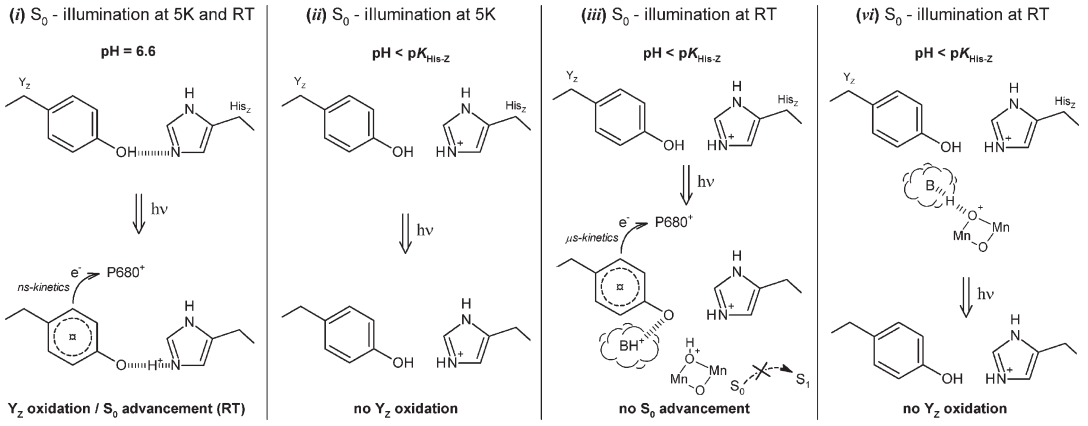

The results will be discussed in context to previously reported pH-dependent inhibitions of S state transitions at room temperature and split EPR signal formations at 5 K (Table 1). But first we should state some prerequisites for our experiments. All experiments were performed on PSII particles with Y_D completely oxidized to avoid competition between Y_Z and Y_D. It has been demonstrated that the rate of Y_D oxidation at room temperature (*45*) and the amount of Y_D oxidation at cryogenic temperatures ($pK_a \sim 7.6$) increases as pH increases (*46*). At this pH ($pK_a \sim 8.0$) Y_D oxidation (in case Y_D was reduced when the illumination started) actually directly competes with the split S_1 EPR signal formation at 5 K (*29*). In order to exclude any possible contribution from oxidized Y_D in the spectra of the fast-decaying radical, the power saturation was measured also at high pH. $P_{1/2}$ was found to be 360 μW at pH 7.6 (Table 2), similar to what was found at pH 6.1, while $P_{1/2}$ for $Y_D^\bullet$ in the S_0 state was 57 μW.

The photooxidation of the alternative electron donors Cyt b_{559}, Chl, and Car can also contribute to P_{680}^+ reduction (*35*, *47*). The amount of the Cyt b_{559} and $Car^{+\bullet}/Chl^{+\bullet}$ induced by our 5 K illumination was estimated over the entire pH range (Figure 4). The induction of $Car^{+\bullet}/Chl^{+\bullet}$ had a minimum at pH 5−7 and increased at both low and high pH. Thus, in accordance with the previous observation in the S_1 state (*29*), a trend is observed also in the S_0 state where the probability for electron donation to P_{680}^+ from the alternative pathways increases when the main pathway via Y_Z is inhibited.

Furthermore, it is also necessary to control irreversible pH-induced damage of the samples. The $CaMn_4$ cluster is prone to be damaged by extreme pH. To overcome this, the remaining PSII activity was evaluated in the same manner as in ref *29* by determining the O_2 evolution at normal pH after the EPR measurements. Any loss of O_2 activity was assigned to PSII centers with a destroyed $CaMn_4$ cluster. These centers do not give rise to a split signal. They are therefore not of interest and were compensated for in our analysis.

From these considerations we argue that the pH-dependent yield of the split S_0 EPR signal and the fast-decaying radical ($Y_Z^\bullet$) both report on the molecular structure in the immediate environment of Y_Z and will be influenced by the distribution of charges and hydrogen bond patterns around $Y_Z^\bullet$. The split S_0 EPR signal is inhibited with the $pK_{app} \sim 4.8$ on the acidic side and $pK_{app} \sim 7.9$ on the alkaline side. The light-induced, fast-decaying radical shows similar pH dependence with the pK_{app}s ~4.8 and ~7.2. The pK_{app} values are extracted from the half-inhibition of the signal, i.e., at 50% of the signal amplitude. This type of apparent pK_a values seems to be more relevant to allow comparisons to previously reported pK_a values (*30*−*32*) and will be used in the discussion (see also Materials and Methods section).

pH Dependence on the Acidic Side. We first discuss the molecular mechanisms behind the acidic pH dependence. It was recently shown that the split S_0 EPR signal decreases with a pK_a of 4.7 at the acidic side (*30*). In our study we include also the fast-decaying radical signal induced at 5 K, and for both signals we find a $pK_{app} \sim 4.8$.

It is likely that the decrease of the split S_0 EPR signal at low pH can be explained in a similar manner as the decrease of the split S_1 EPR signal (*29*) which has a similar pH dependence (*29*, *30*). At optimal pH (pH ~6.6), the hydrogen bond between Y_Z and His_Z is well-defined, allowing oxidation of Y_Z even at 5 K (Scheme 1, i). When decreasing the pH, the mode of the hydrogen bond between Y_Z and His_Z is changed. We propose that the Y_Z-His_Z motif becomes protonated at the N_ε of His_Z (Scheme 1, ii) to form the imidazolium state with a $pK_{app} \sim 4.8$. This low pK_a (for a histidine residue) reflects that the His_Z participates in the H-bond with Y_Z. The pK_{app} for His_Z is similar in the S_1 and S_0 states. This protonation leads to the loss of the essential well-set hydrogen bond necessary for electron donation by Y_Z at cryogenic temperature (*29*) (Scheme 1, ii). Thereby, the oxidation of Y_Z is prevented at low pH, and the amplitude of the split S_0 EPR signal decreases.

Kinetic measurements at room temperature support our conclusions. At physiological pH and temperature, the reduction of P_{680}^+ by Y_Z is proposed to occur in two distinct steps. The first step occurs in the nanosecond time domain reflecting an electron transfer event coupled to non-rate-limiting proton transfer. The second step occurs in the microsecond time domain and represents an overall relaxation within a hydrogen bond network (*9*, *48*). The nanosecond kinetics has, in the lower S states, a low activation energy (50−100 meV) and shows virtually no kinetic H/D isotope effect (*15*, *16*, *49*, *50*). This supports a well set hydrogen bond between Y_Z and the accepting base (His_Z) in the Y_Z-His_Z motif. The amplitude of the nanosecond kinetics decreases at lower pH with a pK_a of 4.5−5.3 (*15*, *17*, *51*−*53*), similar to our $pK_{app} \sim 4.8$ for the decrease of the split S_0 EPR signal. Thus, we conclude that both the fast nanosecond kinetics at physiological temperature and the cryogenic oxidation of Y_Z depend on the well set hydrogen bond between Y_Z and His_Z.

The split S_0 EPR signal induced at 5 K and the $S_0 \rightarrow S_1$ transition at room temperature are inhibited with similar acidic p*K*s ($pK_{app} \sim 4.8$ and $pK_a \sim 4.7$ (*31*, *32*), respectively). This is different from the situation in the S_1 state where the split S_1 EPR

signal formed at 5 K decreases with pK_a ~ 4.7 (*29*) while the $S_1 \rightarrow S_2$ transition at room temperature is pH independent (*31*, *32*).

The difference is useful and allows further dissection of the pH dependence between the $CaMn_4$ cluster and Y_Z in the S_0 state. In this context it is important to realize that Y_Z must be involved in a very well defined hydrogen bond to be oxidized at 5 K. This does not necessarily apply at room temperature where Y_Z can be oxidized with microsecond kinetics when the hydrogen bond to His_Z is not set. In this case Y_Z oxidation probably involves deprotonation to another base, B. This situation was proposed to apply for Y_Z in the S_1 state (*29*), explaining the apparent contradiction that the $S_1 \rightarrow S_2$ transition is pH independent at room temperature while Y_Z oxidation was inhibited with pK_a ~ 4.7 at 5 K.

The situation is obviously different in the S_0 state where the inhibition with pK_{app} ~ 4.8 of Y_Z oxidation at 5 K indicates that the hydrogen bond to His_Z is broken, presumably by protonation of His_Z. This situation is depicted in Scheme 1 panel ii. If Y_Z−OH is involved in a weaker hydrogen bond to base B (as proposed in the S_1 state (*29*)), the situation in Scheme 1 panel iii would prevail. In this case, oxidation of Y_Z at room temperature would occur at low pH, and the observed inhibition of the $S_0 \rightarrow S_1$ transition must occur at the level of the $CaMn_4$ cluster (Scheme 1, iii). A possible scenario in this situation is that the inhibition of the $CaMn_4$ cluster (pK_a ~ 4.7) occurs at a base that would accept the proton that is released in the $S_0 \rightarrow S_1$ transition. It is likely that the same base that promotes deprotonation of Y_Z, B (Scheme 1, iii), is involved (the same pK_as are involved). In this situation the base is inactivated for proton transfer from the $CaMn_4$ cluster since B is already occupied by forming a hydrogen bond to Y_Z.

An alternative scenario can also explain our data (Scheme 1, iv). Here the proton that is to be expelled from the $CaMn_4$ cluster in the $S_0 \rightarrow S_1$ transition already forms a hydrogen bond to B before the photon arrives. In this situation B is no longer available as a proton acceptor for Y_Z−OH, and this lack of available base prevents Y_Z oxidation. Further experimentation is needed to discriminate between these two possibilities.

Our data provide no information of the identity of the base B in Scheme 1. However, interesting candidates for the base B involve the close-lying D1-Glu189 and/or water molecule(s) thought to be present in the ligand sphere around the Ca^{2+} ion (*24*, *25*, *54*). All of those are found within a distance of a few angstroms from Y_Z-OH (*24*, *25*).

pH Dependence on the Alkaline Side. It was earlier reported that the split S_0 EPR signal decreases on the alkaline pH side with the pK_a ~ 7.7 (*30*). This is similar to the pK_{app} 7.9 we report here for the decrease of the split S_0 EPR signal. We extend this observation to the light-induced, fast-decaying radical. This shows a complex pH dependence at alkaline pH. Between pH 6.6 and pH 7.7 the pH dependence of the fast-decaying radical (Figure 3B, closed circles) and the split S_0 EPR signal (Figure 3B, open circles) is nearly identical. However, at pH >7.7, the fast-decaying radical is stabilized at 50−70% of its maximal amplitude. It is likely that this reflects different mechanisms for the decrease of the split S_0 EPR signal at pH below ~7.7 and pH above ~7.7. We will first discuss the pH dependence at pH <7.7.

By increasing the pH it is expected that the hydrogen bond network around Y_Z and His_Z (the Y_Z-His_Z motif) which is quite accessible to the pH (*29*−*33*, *55*) becomes partially deprotonated. A recent FTIR study shows that Y_D on the D2 protein remains protonated in its reduced form between pH 6 and pH 10 (*56*). If this holds true also for Y_Z, oxidation at alkaline pH also must involve a proton movement in a hydrogen bond. A change in the hydrogen bond network around Y_Z at alkaline pH might not significantly affect electron transfer at room temperature as indicated by the pH-independent $S_0 \rightarrow S_1$ transition (*31*, *32*) and the pH-independent nanosecond kinetics in the alkaline region. However, a destabilized hydrogen bond in the Y_Z-His_Z motif due to deprotonation of a supporting hydrogen bond network is likely to show up at 5 K. We suggest that a deprotonation around Y_Z-His_Z is the reason for the decrease between pH 6.6 and pH 7.7 observed for the split S_0 EPR signal and the fast-decaying radical.

Structural changes caused by deprotonation in the immediate surroundings of Y_Z are supported in kinetic measurements. The probability of the so-called misses in oxygen evolution increases at both low and high pH (*15*). The increase at low pH can be explained by protonation of His_Z (see above) leading to dominating microsecond kinetics for P_{680}^+ reduction by Y_Z. Thereby, the misses will increase due to increased recombination between P_{680}^+ and Q_A^-. By comparing the extent of turnover misses in D_2O and H_2O, it was suggested that the presence of the heavier D_2O retards the relaxation process in the H-bond network at low pH (*15*, *48*). However, at alkaline pH, pL >7.0, the fraction of misses was lower in D_2O than in H_2O (*15*). Therefore, the mechanism for the increased misses at high pH must be different from the retardation of Y_Z oxidation causing the increased misses at low pH. Instead, structural changes induced by deprotonations of several weak acids in the hydrogen bond network were suggested to occur at pH >7.0. This is comparable to the concerted decrease of the split S_0 EPR signal and the fast-decaying radical that we observe at pH 6.6−7.7.

At pH 7.7−8.2 the amplitude of the fast-decaying radical is pH independent while the split S_0 EPR signal decreases significantly (Figure 3B). As discussed above, we hypothesize that the fast-decaying radical reflects $Y_Z^\bullet$ in PSII centers where Y_Z and the $CaMn_4$ cluster are magnetically uncoupled. Since the fast-decaying radical is pH independent at pH 7.7−8.2, we suggest that the decrease of the split S_0 EPR signal at pH >7.7 reflects pH-induced changes on the $CaMn_4$ cluster instead of a decrease in Y_Z oxidation.

The decrease of the split S_0 EPR signal at pH >7.7 occurs concomitantly with the appearance of a new, light-induced, broadened EPR signal (Figure 1B, open circles) which is formed with a pK_{app} close to 8. The exact nature of this new EPR signal cannot be ascertained at this early stage. It bears resemblance with the split signals, is fast relaxing, and decays in a few minutes at 5 K. We propose that this new EPR feature in fact reflects a changed interaction signal between $Y_Z^\bullet$ and the $CaMn_4$ cluster caused by a changed Mn coupling within the cluster itself. There is precedence for pH-induced magnetic changes in the $CaMn_4$ cluster in the S_0 state (*33*). The S_0 multiline signal was found to disappear with pK_a ~ 8.0 at alkaline pH. The disappearance was reversible, and the S_0 multiline signal reappeared when the pH was brought back from pH 8.6 to pH 6.2 (*33*). This indicates that the S_0 state was still present at elevated pH, and the observed loss of the S_0 multiline signal was explained by changes in the magnetic coupling within the $CaMn_4$ cluster, e.g., due to deprotonation of an oxo bridge (*31*−*33*). In the same way as the amplitude of the S_0 state multiline signal was recovered if the pH was changed back, the signal shape of the split S_0 EPR signal is recovered to the 160 G separated peaks when the pH is reversed (Figure 5A). Thus, we suggest that a pH >8.0 in the S_0 state

changes the magnetic couplings within the $CaMn_4$ cluster. This modifies the magnetic coupling to $Y_Z^{\bullet}$ which is observed as a new EPR signal.

Mechanistic Implications to pK_{app} of His_Z. It is important to discuss the assignment of $pK_{app} \sim 4.8$ to protonation of His_Z in the Y_Z-His_Z motif. Table 3 describes a series of pK_as that have been assigned to titration of the bases forming the hydrogen bonds to Y_Z or Y_D, respectively (now known to be His_Z and His_D on the D1 and D2 proteins, respectively). A $pK_a \sim 7.3-7.5$ for electron transfer between Y_D and the $CaMn_4$ cluster was early proposed to reflect titration of His_D (*57*). This was the first experimental assignment of this important hydrogen bond. In later studies, cryogenic oxidation of Y_D both in intact and in Mn-depleted PSII was found to increase with a $pK_a \sim 7.6-8.0$, also suggested to reflect titration of His_D (*29*, *46*). Thus, there is consensus that His_D in the Y_D-His_D motif on the D2 protein has a pK_a of ca. 7.6−8.0 that steers oxidation of Y_D. Importantly, this pK_a is essentially insensitive to the presence or absence of the $CaMn_4$ cluster.

Table 3: pK_a Values Measured in Mn-Depleted or Intact PSII Preparations That Can Be Assigned to His_D and His_Z

		~pK_a	ref
His_D	intact	7.3−7.5	*57*
	intact[a]	8.0	*29*
	Mn-depleted[a]	7.6	*46*
His_Z	dark grown[b]	7.6	*11*
	Mn-depleted	6.9−7.5	(*17*, *58*, *59*)
	intact	4.5−5.3	(*15*, *17*, *52*, *53*, *60*)
	intact[a]	4.7−4.9	this work,[c] (*29*, *30*)

[a]Measured at cryogenic temperature. [b]Measured in dark grown *C. reinhardtii*. [c]pK_{app} (see Materials and Methods).

The situation is different around Y_Z, and two systems have been investigated. His_Z has been assigned a $pK_a \sim 7.6$ in PSII from dark grown *Chlamydomonas reinhardtii* where the $CaMn_4$ cluster is absent (*11*). A similar pK_a (~7.0 (*17*), 6.9−7.5 (*58*)) was assigned to His_Z in PSII cores where the $CaMn_4$ cluster was removed. It can thus be concluded that His_D and His_Z in the absence of the $CaMn_4$ cluster are quite similar and that they titrate with quite similar pK_as. The pK_a of His_Z changes dramatically when the $CaMn_4$ cluster is present. This was observed in early studies of P_{680}^+ reduction in Tris-washed (*59*) and intact chloroplasts (*60*) although the observed kinetics could not be assigned molecularly since the identity of neither Y_Z nor His_Z was known (Table 3). Since then, kinetic measurements at room temperature and EPR measurements at cryogenic temperature in both the S_0 and S_1 states have reported a pK_a of 4.5−5.3 (*15*, *17*, *29*, *30*, *52*, *53*) (Table 3). It can thus be concluded that the presence of the $CaMn_4$ cluster steers the protonation/deprotonation of His_Z very efficiently presumably by Coulombic effects.

This is important for the function of the OEC! If the pK_a of His_Z was high, the important hydrogen bond between Y_Z and His_Z would not be sufficiently well-defined at physiological pH to allow Y_Z oxidation with fast nanosecond kinetics. This would lead to increased misses, slower reduction of P_{680}^+, and presumably faster photoinhibition of PSII.

A last interesting consequence of these effects of the $CaMn_4$ cluster on the hydrogen bond between Y_Z and His_Z concerns several observations of changes on the donor and acceptor side of PSII that occur simultaneously and are correlated to a defined chemical perturbation of the OEC. It is known that for example Ca^{2+} depletion, removal of the $CaMn_4$ cluster, or extrinsic subunits in PSII induces changes in the redox potential of Q_A (and perhaps Q_B) and Cyt b_{559}, in electron transfer from Q_A^-,

Scheme 2: Structural Rearrangements of Helix C and Helix D Translating Changes from the Donor to the Acceptor Side of PSII at pH ~6[a]

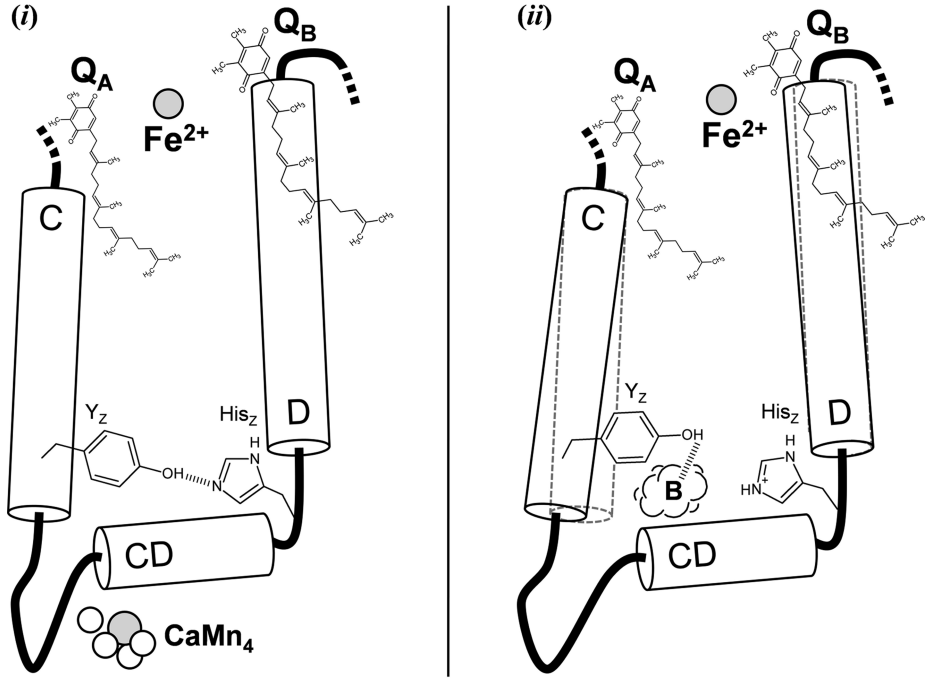

[a]In the presence of the $CaMn_4$ cluster the hydrogen bond in the Y_Z-His_Z motif is well set (i). In the absence of the $CaMn_4$ cluster the hydrogen bond between Y_Z and His_Z is broken, and a base (B) is involved in a hydrogen bond to Y_Z instead (ii). This might provoke slight movements of helices C and D that transplant through the membrane affecting Q_A and/or Q_B.

etc. This is thought to reflect translation of a change in the OEC to the distant redox cofactors on the other side of the thylakoid membrane through unidentified structural reorganizations. The breaking and resetting of the hydrogen bond between Y_Z and His_Z on the D1 protein represent the first identification of a structural change that could transplant from one side of PSII to the other (Scheme 2).

Y_Z is located to the lumenal end of the membrane-spanning helix C in the D1 protein while His_Z is found in a short loop connecting the membrane parallel CD helix and the membrane-spanning helix D. When the $CaMn_4$ cluster is present, Y_Z and His_Z form the hydrogen bond at physiological pH, and helices C and D take the positions observed in the X-ray structures of PSII (*24*, *25*). However, when the $CaMn_4$ cluster is absent, the hydrogen bond is broken since His_Z is protonated at physiological pH. Our data imply a base (B in Schemes 1 and 2) that will involve Y_Z-OH in this situation. The formation of this new hydrogen bond and the breaking of the well-defined Y_Z-His_Z hydrogen bond will certainly induce a structural rearrangement of Y_Z. It is not at all unlikely that this will involve a (small) movement of helix C relative to helix D. Since both helices are membrane spanning, this could translate into altered structures around the quinone acceptors (mainly Q_B and the acceptor side Fe^{2+}, Scheme 2). These are all close to the stromal ends of D1-helices C and D. It is tempting to speculate that similar helix movements, involving D2-helices C and D (not shown) could be induced by the making and breaking of the corresponding hydrogen bond between Y_D and His_D on the D2 protein. In this case, the helix movements would presumably influence the structures around Q_A and the acceptor side Fe^{2+}.

CONCLUSIONS

The double nature of the $S_0Y_Z^{\bullet}$ magnetic interaction signal (split S_0) becomes evident from our investigation of its pH dependence, reporting on changes around Y_Z and within the $CaMn_4$ cluster. We observed three separate proton-steered mechanistic effects reflected in the pH dependence of the split signal induction: (i) At acidic pH, Y_Z oxidation at 5 K is blocked, probably by protonation of His_Z that inhibits the formation of the well-tuned H-bond to Y_Z necessary for proton-coupled electron transfer to occur at this low temperature (*29*). (ii) At moderate alkaline pH (7.0−7.7), Y_Z oxidation at 5 K seems to be less efficient. The reason for this is proposed to reflect deprotonation of the stabilizing hydrogen bond network around Y_Z that functions to maintain the position of the essential Y_Z-His_Z hydrogen bond. (iii) At pH >7.7 the continued decrease of the 160 G wide split S_0 EPR signal and the appearance of the new broadened $g \sim 2$ EPR feature is most likely connected to magnetic changes in the $CaMn_4$ cluster itself, tentatively assigned to be caused by deprotonation of the protonated μ-oxo bridge present in the S_0 state (*33*, *61*, *62*).

ACKNOWLEDGMENT

Valuable discussions with Dr. Felix Ho and Dr. Anders Thapper are gratefully acknowledged.

REFERENCES

1. Barber, J. (2003) Photosystem II: The engine of life. *Q. Rev. Biophys. 36*, 71–89.
2. Dau, H., and Haumann, M. (2007) Eight steps preceding O-O bond formation in oxygenic photosynthesis—A basic reaction cycle of the photosystem II manganese complex. *Biochim. Biophys. Acta 1767*, 472–483.
3. McEvoy, J. P., and Brudvig, G. W. (2006) Water-splitting chemistry of photosystem II. *Chem. Rev. 106*, 4455–4483.
4. Noguchi, T., Inoue, Y., and Tang, X. S. (1997) Structural coupling between the oxygen-evolving Mn cluster and a tyrosine residue in photosystem II as revealed by Fourier transform infrared spectroscopy. *Biochemistry 36*, 14705–14711.
5. Berthomieu, C., Hienerwadel, R., Boussac, A., Breton, J., and Diner, B. A. (1998) Hydrogen bonding of redox-active tyrosine Z of photosystem II probed by FTIR difference spectroscopy. *Biochemistry 37*, 10547–10554.
6. Tommos, C., Tang, X. S., Warncke, K., Hoganson, C. W., Styring, S., McCracken, J., Diner, B. A., and Babcock, G. T. (1995) Spin-density distribution, conformation, and hydrogen-bonding of the redox-active tyrosine Y_Z in photosystem II from multiple electron magnetic-resonance spectroscopies: Implications for photosynthetic oxygen evolution. *J. Am. Chem. Soc. 117*, 10325–10335.
7. Brettel, K., Schlodder, E., and Witt, H. T. (1984) Nanosecond reduction kinetics of photooxidized chlorophyll-a_{II} (P-680) in single flashes as a probe for the electron pathway, H^+-release and charge accumulation in the O_2-evolving complex. *Biochim. Biophys. Acta 766*, 403–415.
8. Christen, G., Reifarth, F., and Renger, G. (1998) On the origin of the "35-μs kinetics" of $P680^{+\bullet}$ reduction in photosystem II with an intact water oxidising complex. *FEBS Lett. 429*, 49–52.
9. Schilstra, M. J., Rappaport, F., Nugent, J. H. A., Barnett, C. J., and Klug, D. R. (1998) Proton/hydrogen transfer affects the S state-dependent microsecond phases of $P680^+$ reduction during water splitting. *Biochemistry 37*, 3974–3981.
10. Rappaport, F., Blanchard-Desce, M., and Lavergne, J. (1994) Kinetics of electron transfer and electrochromic change during the redox transitions of the photosynthetic oxygen-evolving complex. *Biochim. Biophys. Acta 1184*, 178–192.
11. Mamedov, F., Sayre, R. T., and Styring, S. (1998) Involvement of histidine 190 on the D1 protein in electron/proton transfer reactions on the donor side of photosystem II. *Biochemistry 37*, 14245–14256.
12. Hays, A. M. A., Vassiliev, I. R., Golbeck, J. H., and Debus, R. J. (1998) Role of D1-His190 in proton-coupled electron transfer reactions in photosystem II: A chemical complementation study. *Biochemistry 37*, 11352–11365.
13. Hoganson, C. W., Lydakis-Simantiris, N., Tang, X. S., Tommos, C., Warncke, K., Babcock, G. T., Diner, B. A., McCracken, J., and Styring, S. (1995) A hydrogen-atom abstraction model for the function of Y_Z in photosynthetic oxygen evolution. *Photosynth. Res. 46*, 177–184.
14. Hoganson, C. W., and Babcock, G. T. (1997) A metalloradical mechanism for the generation of oxygen from water in photosynthesis. *Science 277*, 1953–1956.
15. Christen, G., Seeliger, A., and Renger, G. (1999) $P680^{+\bullet}$ reduction kinetics and redox transition probability of the water oxidizing complex as a function of pH and H/D isotope exchange in spinach thylakoids. *Biochemistry 38*, 6082–6092.
16. Eckert, H. J., and Renger, G. (1988) Temperature dependence of $P680^+$ reduction in O_2-evolving PS II membrane-fragments at different redox states S_i of the water oxidizing system. *FEBS Lett. 236*, 425–431.
17. Ahlbrink, R., Haumann, M., Cherepanov, D., Bogershausen, O., Mulkidjanian, A., and Junge, W. (1998) Function of tyrosine Z in water oxidation by photosystem II: Electrostatical promotor instead of hydrogen abstractor. *Biochemistry 37*, 1131–1142.
18. Junge, W., Haumann, M., Ahlbrink, R., Mulkidjanian, A., and Clausen, J. (2002) Electrostatics and proton transfer in photosynthetic water oxidation. *Philos. Trans. R. Soc. London, Ser. B 357*, 1407–1417.
19. Styring, S., and Rutherford, A. W. (1988) Deactivation kinetics and temperature-dependence of the S-state transitions in the oxygen-evolving system of photosystem II measured by EPR spectroscopy. *Biochim. Biophys. Acta 933*, 378–387.
20. Nugent, J. H., Muhiuddin, I. P., and Evans, M. C. (2002) Electron transfer from the water oxidizing complex at cryogenic temperatures: the S_1 to S_2 step. *Biochemistry 41*, 4117–4126.
21. Zhang, C., and Styring, S. (2003) Formation of split electron paramagnetic resonance signals in photosystem II suggests that $tyrosine_Z$ can be photooxidized at 5 K in the S_0 and S_1 states of the oxygen-evolving complex. *Biochemistry 42*, 8066–8076.
22. Zhang, C., Boussac, A., and Rutherford, A. W. (2004) Low-temperature electron transfer in photosystem II: A tyrosyl radical and semiquinone charge pair. *Biochemistry 43*, 13787–13795.

23. Havelius, K. G. V., Su, J. H., Feyziyev, Y., Mamedov, F., and Styring, S. (2006) Spectral resolution of the split EPR signals induced by illumination at 5 K from the S_1, S_3, and S_0 states in photosystem II. *Biochemistry 45*, 9279–9290.
24. Ferreira, K. N., Iverson, T. M., Maghlaoui, K., Barber, J., and Iwata, S. (2004) Architecture of the photosynthetic oxygen-evolving center. *Science 303*, 1831–1838.
25. Loll, B., Kern, J., Saenger, W., Zouni, A., and Biesiadka, J. (2005) Towards complete cofactor arrangement in the 3.0 Å resolution structure of photosystem II. *Nature 438*, 1040–1044.
26. Debus, R. J. (1992) The manganese and calcium ions of photosynthetic oxygen evolution. *Biochim. Biophys. Acta 1102*, 269–352.
27. Petrouleas, V., Koulougliotis, D., and Ioannidis, N. (2005) Trapping of metalloradical intermediates of the S-states at liquid helium temperatures. Overview of the phenomenology and mechanistic implications. *Biochemistry 44*, 6723–6728.
28. Su, J. H., Havelius, K. G. V., Ho, F. M., Han, G., Mamedov, F., and Styring, S. (2007) Formation spectra of the EPR split signals from the S_0, S_1, and S_3 states in photosystem II induced by monochromatic light at 5 K. *Biochemistry 46*, 10703–10712.
29. Havelius, K. G., and Styring, S. (2007) pH dependent competition between Y_Z and Y_D in photosystem II probed by illumination at 5 K. *Biochemistry 46*, 7865–7874.
30. Zhang, C. (2006) Interaction between tyrosine$_Z$ and substrate water in active photosystem II. *Biochim. Biophys. Acta 1757*, 781–786.
31. Bernat, G., Morvaridi, F., Feyziyev, Y., and Styring, S. (2002) pH dependence of the four individual transitions in the catalytic S-cycle during photosynthetic oxygen evolution. *Biochemistry 41*, 5830–5843.
32. Suzuki, H., Sugiura, M., and Noguchi, T. (2005) pH dependence of the flash-induced S-state transitions in the oxygen-evolving center of photosystem II from *Thermosynechoccocus elongatus* as revealed by Fourier transform infrared spectroscopy. *Biochemistry 44*, 1708–1718.
33. Geijer, P., Deak, Z., and Styring, S. (2000) Proton equilibria in the manganese cluster of photosystem II control the intensities of the S_0 and S_2 state $g \sim 2$ electron paramagnetic resonance signals. *Biochemistry 39*, 6763–6772.
34. Han, G., Ho, F. M., Havelius, K. G. V., Morvaridi, S. F., Mamedov, F., and Styring, S. (2008) Direct quantification of the four individual S states in photosystem II using EPR spectroscopy. *Biochim. Biophys. Acta 1777*, 496–503.
35. Hanley, J., Deligiannakis, Y., Pascal, A., Faller, P., and Rutherford, A. W. (1999) Carotenoid oxidation in photosystem II. *Biochemistry 38*, 8189–8195.
36. Miller, A.-F., and Brudvig, G. W. (1991) A guide to electron paramagnetic resonance spectroscopy of photosystem II membranes. *Biochim. Biophys. Acta 1056*, 1–18.
37. Tracewell, C. A., and Brudvig, G. W. (2003) Two redox-active β-carotene molecules in photosystem II. *Biochemistry 42*, 9127–9136.
38. Styring, S. A., and Rutherford, A. W. (1988) The microwave-power saturation of signal II_{slow} varies with the redox state of the oxygen-evolving complex in photosystem-II. *Biochemistry 27*, 4915–4923.
39. Peterson, S., Ahrling, K. A., and Styring, S. (1999) The EPR signals from the S_0 and S_2 states of the Mn cluster in photosystem II relax differently. *Biochemistry 38*, 15223–15230.
40. Andreasson, L. E., Vass, I., and Styring, S. (1995) Ca^{2+} depletion modifies the electron-transfer on both donor and acceptor sides in photosystem-II from spinach. *Biochim. Biophys. Acta 1230*, 155–164.
41. Su, J. H., Havelius, K. G. V., Mamedov, F., Ho, F. M., and Styring, S. (2006) Split EPR signals from photosystem II are modified by methanol, reflecting S state-dependent binding and alterations in the magnetic coupling in the $CaMn_4$ cluster. *Biochemistry 45*, 7617–7627.
42. Evelo, R. G., Styring, S., Rutherford, A. W., and Hoff, A. J. (1989) EPR relaxation measurements of photosystem II reaction centers—Influence of S-state oxidation and temperature. *Biochim. Biophys. Acta 973*, 428–442.
43. Szalai, V. A., Kühne, H., Lakshmi, K. V., and Brudvig, G. W. (1998) Characterization of the interaction between manganese and tyrosine Z in acetate-inhibited photosystem II. *Biochemistry 37*, 13594–13603.
44. Zahariou, G., Ioannidis, N., Sioros, G., and Petrouleas, V. (2007) The collapse of the tyrosine $Z^{\bullet}$−Mn spin-spin interaction above ~100 K reveals the spectrum of tyrosine $Z^{\bullet}$. An application of rapid-scan EPR to the study of intermediates of the water splitting mechanism of photosystem II. *Biochemistry 46*, 14335–14341.
45. Faller, P., Debus, R. J., Brettel, K., Sugiura, M., Rutherford, A. W., and Boussac, A. (2001) Rapid formation of the stable tyrosyl radical in photosystem II. *Proc. Natl. Acad. Sci. U.S.A. 98*, 14368–14373.
46. Faller, P., Rutherford, A. W., and Debus, R. J. (2002) Tyrosine D oxidation at cryogenic temperature in photosystem II. *Biochemistry 41*, 12914–12920.
47. Tracewell, C. A., Cua, A., Stewart, D. H., Bocian, D. F., and Brudvig, G. W. (2001) Characterization of carotenoid and chlorophyll photooxidation in photosystem II. *Biochemistry 40*, 193–203.
48. Christen, G., and Renger, G. (1999) The role of hydrogen bonds for the multiphasic $P680^{+\bullet}$ reduction by Y_Z in photosystem II with intact oxygen evolution capacity. Analysis of kinetic H/D isotope exchange effects. *Biochemistry 38*, 2068–2077.
49. Jeans, C., Schilstra, M. J., and Klug, D. R. (2002) The temperature dependence of $P680^+$ reduction in oxygen-evolving photosystem II. *Biochemistry 41*, 5015–5023.
50. Karge, M., Irrgang, K. D., Sellin, S., Feinaugle, R., Liu, B., Eckert, H. J., Eichler, H. J., and Renger, G. (1996) Effects of hydrogen deuterium exchange on photosynthetic water cleavage in PS II core complexes from spinach. *FEBS Lett. 378*, 140–144.
51. Schlodder, E., and Meyer, B. (1987) pH-dependence of oxygen evolution and reduction kinetics of photooxidized chlorophyll-a_{II} (P-680) in photosystem II particles from *Synechococcus* sp. *Biochim. Biophys. Acta 890*, 23–31.
52. Meyer, B., Schlodder, E., Dekker, J. P., and Witt, H. T. (1989) O_2 evolution and Chl-a_{II}^+ ($P\text{-}680^+$) nanosecond reduction kinetics in single flashes as a function of pH. *Biochim. Biophys. Acta 974*, 36–43.
53. Kühn, P., Pieper, J., Kaminskaya, O., Eckert, H. J., Lechner, R. E., Shuvalov, V., and Renger, G. (2005) Reaction pattern of photosystem II: Oxidative water cleavage and protein flexibility. *Photosynth. Res. 84*, 317–323.
54. Chu, H.-A., Nguyen, A. P., and Debus, R. J. (2002) Amino acid residues that influence the binding of manganese or calcium to photosystem II. 1. The lumenal interhelical domains of the D1 polypeptide. *Biochemistry 34*, 5839–5858.
55. Svensson, B., Vass, I., and Styring, S. (1991) Sequence analysis of the D1 and D2 reaction center proteins of photosystem II. *Z. Naturforsch. C 46*, 765–776.
56. Hienerwadel, R., Diner, B. A., and Berthomieu, C. (2008) Molecular origin of the pH dependence of tyrosine D oxidation kinetics and radical stability in photosystem II. *Biochim. Biophys. Acta 1777*, 525–531.
57. Vass, I., and Styring, S. (1991) pH-dependent charge equilibria between tyrosine-D and the S states in photosystem II. Estimation of relative midpoint redox potentials. *Biochemistry 30*, 830–839.
58. Hays, A. M. A., Vassiliev, I. R., Golbeck, J. H., and Debus, R. J. (1999) Role of D1-His190 in the proton-coupled oxidation of tyrosine Y_Z in manganese-depleted photosystem II. *Biochemistry 38*, 11851–11865.
59. Conjeaud, H., and Mathis, P. (1980) The effect of pH on the reduction kinetics of P-680 in tris-treated chloroplasts. *Biochim. Biophys. Acta 590*, 353–359.
60. Renger, G., Gläser, M., and Buchwald, H. E. (1977) The control of the reduction kinetics in the dark of photooxidized chlorophyll a_{II}^+ by the inner thylakoid proton concentration. *Biochim. Biophys. Acta 461*, 392–402.
61. Haumann, M., Muller, C., Liebisch, P., Iuzzolino, L., Dittmer, J., Grabolle, M., Neisius, T., Meyer-Klaucke, W., and Dau, H. (2005) Structural and oxidation state changes of the photosystem II manganese complex in four transitions of the water oxidation cycle ($S_0 \rightarrow S_1$, $S_1 \rightarrow S_2$, $S_2 \rightarrow S_3$, and $S_{3,4} \rightarrow S_0$) characterized by X-ray absorption spectroscopy at 20 K and room temperature. *Biochemistry 44*, 1894–1908.
62. Robblee, J. H., Messinger, J., Cinco, R. M., McFarlane, K. L., Fernandez, C., Pizarro, S. A., Sauer, K., and Yachandra, V. K. (2002) The Mn cluster in the S_0 state of the oxygen-evolving complex of photosystem II studied by EXAFS spectroscopy: Are there three di-μ oxo-bridged Mn_2 moieties in the tetranuclear Mn complex? *J. Am. Chem. Soc. 124*, 7459–7471.